



Article

Dynamic Nucleation in Zr-2.5Nb During Reduced-Gravity Electromagnetic Levitation Experiments

Gwendolyn P. Bracker ^{1,2,*} , Stephan Schneider ² , Sarah Nell ², Mitja Beckers ², Markus Mohr ^{3,4} and Robert W. Hyers ¹

¹ Department of Mechanical and Materials Engineering, Worcester Polytechnic Institute, Worcester, MA 01609, USA; rwhyers@wpi.edu

² Institute for Frontier Materials on Earth and in Space, German Aerospace Center (DLR), 51147 Köln, Germany

³ Institute of Functional Nanosystems, Ulm University, 89081 Ulm, Germany

⁴ Institute of Quantum Technologies, German Aerospace Center (DLR), 89081 Ulm, Germany

* Correspondence: gbracker@wpi.edu

Abstract

Levitation techniques reduce the available heterogeneous nucleation sites and provide stable access to deeply undercooled melts. However, some samples have repeatably demonstrated that, in the presence of strong stirring, solidification may be induced at moderate, sub-critical undercoolings. Dynamic nucleation is a mechanism by which solidification may be induced through flow effects within a sub-critically undercooled melt. In this mechanism, collapsing cavities within the melt produce very high-pressure shocks, which shift the local melting temperature. In these regions of locally shifted melt temperatures, thermodynamic conditions enable nuclei to grow and trigger solidification of the full sample. By deepening the local undercooling, dynamic nucleation enables solidification to occur in conditions where classical nucleation does not. Dynamic nucleation has been observed in several zirconium and zirconium-based samples in the Electromagnetic Levitator onboard the International Space Station (ISS-EML). The experiments presented here address conditions in which a zirconium sample alloyed with 2.5 atomic percent niobium spontaneously solidifies during electromagnetic levitation experiments with strong melt stirring. In these experimental conditions, classical nucleation predicts the sample to remain liquid. This solidification behavior is consistent with the solidification behavior observed in prior experiments on pure zirconium.

Keywords: dynamic nucleation; undercooled melts; electromagnetic levitation; ISS-EML; magnetohydrodynamic modeling



Academic Editor: Jan Macutkevici

Received: 2 July 2025

Revised: 25 July 2025

Accepted: 29 July 2025

Published: 31 July 2025

Citation: Bracker, G.P.; Schneider, S.; Nell, S.; Beckers, M.; Mohr, M.; Hyers, R.W. Dynamic Nucleation in Zr-2.5Nb During Reduced-Gravity Electromagnetic Levitation Experiments. *Crystals* **2025**, *15*, 703. <https://doi.org/10.3390/cryst15080703>

Copyright: © 2025 by the authors. Licensee MDPI, Basel, Switzerland. This article is an open access article distributed under the terms and conditions of the Creative Commons Attribution (CC BY) license (<https://creativecommons.org/licenses/by/4.0/>).

1. Introduction

Containerless processing techniques, such as electrostatic levitation (ESL) and electromagnetic levitation (EML), eliminate the interface between a melt and its container. In electromagnetic levitation, a high-frequency, alternating electrical current flowing through a coil system induces a magnetic field. This magnetic field supports the sample through Lorentz forces and heats the sample via Joule heating. In the absence of a solid–liquid interface, the opportunity for contamination and available heterogeneous nucleation sites are reduced, which provides greater access to the melt in the undercooled state for investigation. Recent experiments using EML include studies on the structure of liquids [1,2], solidification front velocities [3–5], phase transformations [6], rapid solidification [7,8], the fundamentals of nucleation [9], fluid flow [10], and thermophysical properties [11–13].

During levitation, undercooled liquids are expected to be very stable and have been shown to achieve undercoolings as deep as 18% of the absolute melting temperature of a sample [14]. Despite the expected stability in liquid, some EML experiments experienced unexpected solidification events which were attributed to cavitating flow effects. Cavitating flow requires very high flow rates at a reduced pressure; while EML experiments can have strong stirring, the induced flow rates are well below the flow required to induce cavitation in the melt. Instead, dynamic nucleation relies on exciting voids already existing in the melt. In the first systematic investigation into dynamic nucleation, experiments were confined to flow conditions far below the threshold for cavitation. Yet, the molten sample solidified in 18 of 19 instances, where classical nucleation could not be observed on the laboratory timescale [9]. In the work presented here, the investigation into dynamic nucleation has been expanded to an alloy to reveal the nature of this solidification phenomenon.

In classical nucleation theory, the formation of a new phase is described as a function of competition between the free energy released by crystallization of the new phase and the free energy required to form the interface between phases. The free energy of formation of the solid phase and the energy to form the interface between phases give the system a critical radius of curvature, r^* , required for a nucleus at a given undercooling to be stable. Equation (1) relates the critical radius with the interfacial free energy between phases, γ_{SL} , and the free energy per unit volume released by solidification, ΔG_V .

$$r^* = \frac{2\gamma_{SL}}{\Delta G_V} \quad (1)$$

For nuclei above the critical radius, r^* , it is energetically favorable to grow, meanwhile any sub-critical nuclei will be, on average, dissolving back into the liquid. The free energy required to form a nucleus of critical size, ΔG^* , is described by Equation (2) [15]. Here, L_v is the volumetric latent heat of fusion, T_m is the melting temperature of the solid, and ΔT is the undercooling defined as $T_m - T$.

$$\Delta G^* = \frac{16\pi}{3} \frac{\gamma_{SL}^3 T_m^2}{L_v^2 \Delta T^2} \quad (2)$$

These nuclei are constantly forming and dissolving back into the melt. The rate of formation of these critical nuclei, n_r , is given in Equation (3) as a function of the free energy required to form a critical cluster, ΔG^* , the temperature, T , and the Boltzmann constant k . The prefactor, A , encompasses kinetic factors, including the atomic vibration frequency, the diffusion coefficient in the melt, and the number of atoms per unit volume in the system.

$$n_r = A \times \exp\left(\frac{-\Delta G^*}{kT}\right) \quad (3)$$

The nucleation rate is strongly affected by the temperature of the melt, such that a small temperature change may result in a shift in the nucleation rate by several orders of magnitude. This rapid onset of nucleation and increase in nucleation rate occur at the critical undercooling, which, in metallic melts, has been demonstrated to be up to 18% of the absolute melting temperature [14]. However, at shallower levels of undercoolings, the nucleation rate is very small. Prior work has demonstrated that in pure zirconium, which has a critical undercooling of 334 ± 4 K [16], decreasing the undercooling by 80 K from the critical undercooling temperature reduces the nucleation rate in zirconium by 17 orders of magnitude [9,17].

The lifetime of liquid is inversely proportional to the nucleation rate. Therefore, such a large decrease in the nucleation rate at such a moderate undercooling should propor-

tionally extend the expected lifetime of the liquid. During electromagnetic levitation experiments, moderately undercooled samples are expected to be stable within the liquid phase and, by classical nucleation theory, are never expected to solidify on the laboratory time scale. However, levitated samples have not always displayed such reliable behavior.

In a series of experiments by Hofmeister et al., the critical undercooling for zirconium was demonstrated to be 334 K below its melt temperature of 2128 K in a series of 110 free-cooled melt cycles [16,18,19]. However, when the sample was held isothermally between 30 K and 80 K below the melt temperature, the sample solidified. These anomalous solidification instances were attributed to dynamic nucleation [18], similar to [20,21]. More recently dynamic nucleation was observed during experiments on zirconium and zirconium alloys in the Electromagnetic Levitator onboard the International Space Station (ISS-EML) [9,22].

In dynamic nucleation by the collapse of cavities, a solidification event is the result of a series of stochastic processes that cause a shift in the local undercooling. In the more deeply undercooled region, conditions provide sufficient driving forces, locally, to result in the formation of a supercritical nucleus that solidifies the full sample. A change in melting temperature can also change a sub-critical nucleus into a supercritical nucleus. A shift in the local melting temperature of the system is caused by a local, high-pressure shock, as described by the Clapeyron equation given in Equation (4). The large pressure shift, dP , causes a corresponding shift in the local melting temperature, dT , when the enthalpy of solidification, ΔH_{fus} , is assumed to be constant, and Δv describes the change in molar volume associated with the change in phase.

$$\left(\frac{dP}{dT}\right)_{eq} = \frac{\Delta H_{fus}}{T \Delta v} \quad (4)$$

The local region of high pressure originates with the collapse of pre-existing voids within the melt. Such voids have been shown to exist as unevenly distributed free volume ranging from the atomic scale up to $2000 \mu\text{m}^3$ in volume [23]. When the fluid flow transports a void through a low-pressure region, as occurs in turbulent eddies and regions of low hydrostatic tension, the void expands. Upon exiting the low-pressure region, the cavity is compressed. When the changes in pressure and void size are sufficient, the void may collapse and trigger the necessary shock in the melt to shift the local melting temperature.

Locally, the increased melting temperature results in a proportional increase in the local undercooling, thereby providing larger driving forces for the formation of supercritical nuclei. Once a single nucleus has exceeded the critical nucleation radius, solidification begins and continues, even outside the high-pressure region.

2. Materials and Methods

These experiments explored solidification events at sub-critical undercoolings using a zirconium alloy containing 2.5 atomic percent niobium. The composition of the sample was validated using energy-dispersive X-ray spectroscopy. The oxygen concentration in this sample was below the detection limit and iron was below 0.13 atomic percent in the sample. The composition homogeneity of the sample was specified as better than ± 0.5 atomic percent. The mass of the flight sample used in ISS-EML Batch 3 was 1.1556 g and had a diameter of 6.95 ± 0.02 mm at room temperature [24].

Experiments were processed in the EML facility onboard the International Space Station, known as the ISS-EML. Processing in microgravity reduces the levitation force and corresponding Joule heating sufficiently that undercooling in vacuum is possible, which is necessary to observe dynamic nucleation. The levitation system on the ISS-EML comprises two superposed circuits which allow for independent control of the positioning and heating of a sample. Further details on the facility are available in [25–27].

During experimental cycles, the sample was melted, superheated, and cooled to a moderate undercooling. At the targeted undercooling, the sample was held, isothermally, for up to 600 s, or until recalescence and solidification were observed. Figure 1 shows a typical experimental cycle, in which the sample temperature was measured via optical pyrometry, in black and the telemetry for the control of heating and positioning circuits is reported in red and blue, respectively. In this case, heating began at time = 0 s, which corresponds to a rise in the sample temperature. During heating, the melt plateau began around 6.5 s. Following melting and superheating, the sample was allowed to cool, starting here at 12.0 s, until it reached the desired target temperature, here about 1870 K. At the target temperature, in this case around 17.0 s, the heater was applied to maintain the sample in a quasi-isothermal state until recalescence occurred, here, 4.0 s later. During analysis, the instant of solidification was primarily identified by the temperature rise associated with recalescence and confirmed using the high-speed video of the experiments, in which the emissivity shift that resulted from the phase change was recorded. Following recalescence, the heater was reduced, and the sample was allowed to cool prior to further processing.

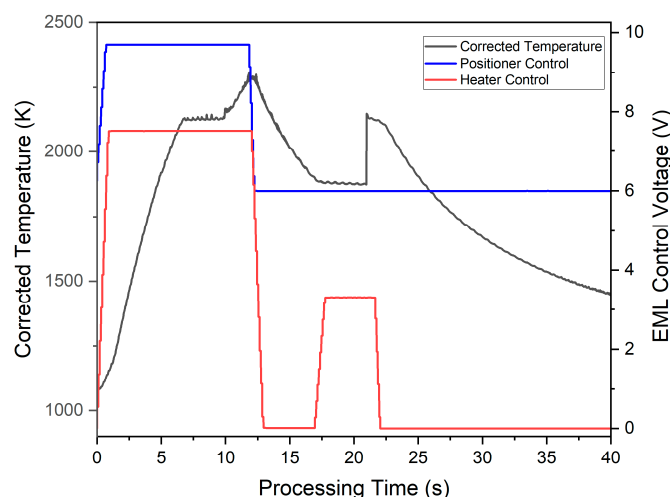


Figure 1. The telemetry data for cycle 46 of Zr-Nb2.5 atomic percent is plotted with the pyrometry given in black and the voltages are overlayed for the positioner circuit in blue and for the heater circuit in red. In this cycle the sample was melted and then held at 255 K below the melting temperature until solidification occurred at $t = 21.0$ s.

Free cooling cycles were run before, midway through, and again at the end of the experiment series to ensure that the sample continued to achieve deep levels of undercooling. In these free cooling cycles, the molten sample was allowed to cool through recalescence, with 0 V applied to the heater circuit. By free-cooling the sample, the maximum undercooling that the sample could achieve in the facility was demonstrated.

Some cycles were stopped during the isothermal hold due to the instability of the sample's center of mass or rotation. For the safety of the facility, the heater was turned off and the sample was allowed to cool and solidify. Once control of the levitation behavior was re-established, processing resumed normally.

3. Results

This experiment series included a total of 30 processing cycles, 1 of which was used to establish the correct camera settings for the experiment, 3 of which were free-cooling cycles, and 26 of which were used to search directly for instances of dynamic nucleation. For these experiments, the sample was cooled to a targeted undercooling and held isothermally between 54 K and 302 K below the melting temperature. The time until solidification is plotted in Figure 2 as a function of the undercooling. In the six cycles, plotted as black Xs,

the sample's levitation behavior required the experiment to be stopped for the safety of the facility. The sample in these halted cycles was still liquid at the time indicated by the X. During this experiment series, spontaneous nucleation events (plotted as blue circles) were observed in 20 of 26 remaining attempts, all in less than 600 s. In no cycles did the sample remain liquid until the end of the allotted experimental time.

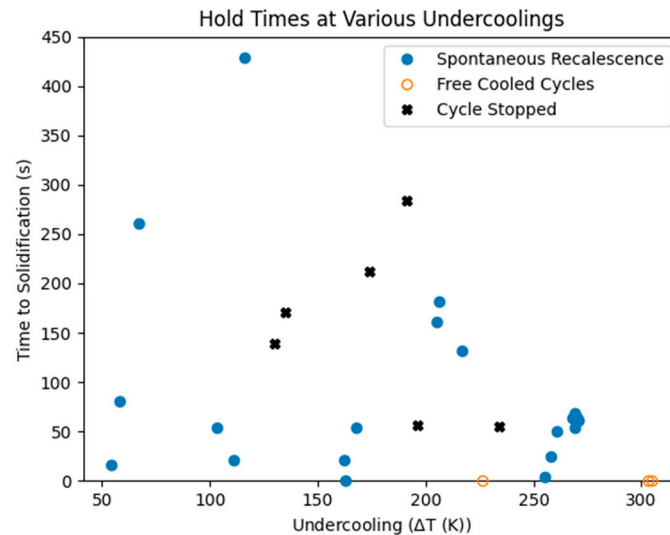


Figure 2. After melting, the liquid Zr-2.5Nb sample was held between 54 and 302 K below the melting temperature. During the isothermal holds, 20 of the 26 cycles experienced a spontaneous nucleation event. The 6 remaining cycles were stopped before the duration of the experiment for the safety of the facility; these halted cycles are indicated with an “x”. In these halted cycles, the sample was still liquid at the indicated time.

Additionally, the observed undercoolings of the free-cooled cycles are plotted with open circles. These free cooling cycles were used to determine the maximum achievable undercooling for this sample. The first two free-cooling cycles cooled to 305 K and 302 K below the melting temperature. The last cycle only cooled to an undercooling of 226 K below the melting temperature; however, the cycle immediately prior was held at 270 K below the melting temperature for over 60 s, which strongly indicates that the sample remained unchanged through the duration of the experiments.

Magnetohydrodynamic modeling was used to calculate the flow within the drop during the isothermal holds. Further details on the magnetohydrodynamic model are available in Appendix A. Magnetohydrodynamic Model, along with vector maps of the magnetic forces, flow patterns during the isothermal holds, and the resulting pressure contours. The thermophysical properties of the liquids were calculated as a function of temperature using the measurements reported in [28]. The results of these calculations are summarized in Figure 3 for different processing conditions.

Void excitation is expected to occur in regions of low pressure which result from the vortices in turbulent eddies, from the fluid flow pattern, or both. Quantifying the turbulence through the Reynolds number and the hydrostatic tension provides an indication of the conditions in which dynamic nucleation is more likely to occur. During the isothermal holds, the flow velocity was calculated to be between 13.8 and 19.4 cm/s, depending on the magnetic field and temperature of the melt. These flows are described by Reynolds numbers between 990 and 1690, plotted with the corresponding hold length in Figure 3a for each of the cycles. In EML samples, the laminar–turbulent transition is known to occur at a Reynolds number of 600 [29], given as a solid line on the left-hand side of the plot in Figure 3a. In all the isothermal holds, the flow exceeded the turbulent transition into turbulent flow. The rapid magnetohydrodynamic flow induced hydrostatic tension in the

melt, as plotted in Figure 3b. During these holds, the deepest hydrostatic tension from the primary flow occurred where the flow was fastest and was between 137 and 235 Pa. It is within these regions of hydrostatic tension that, when combined with the additional hydrostatic tension of a turbulent eddy, void excitation and dynamic nucleation initiation are most likely to occur.

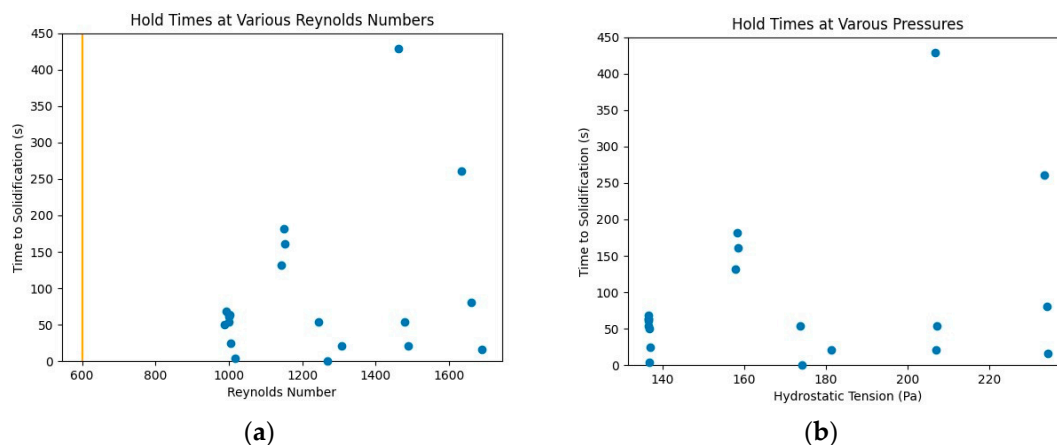


Figure 3. The flow conditions during the isothermal holds are calculated for the experimental parameters in which spontaneous nucleation was observed. (a) The Reynolds numbers describing the fluid flow are all well above the laminar–turbulent transition, indicated by the orange line at $Re = 600$, during the isothermal holds. (b) During the isothermal holds, the rapid fluid flow drives hydrostatic tension. The free-cooling cycles are off to the left of both figures and showed no dynamic nucleation events.

Unlike the isothermal holds, the free-cooling cycles reached much deeper levels of undercooling, which resulted in the liquid being significantly more viscous. During free cooling, the electromagnetic force from the heating circuit was also much weaker than in the isothermal holds. Consequently, the flow speed was much slower, in the order of 6 cm/s, and was described by a Reynolds number of 430. In these conditions the deepest hydrostatic tension in the sample was only 18 Pa, around an order of magnitude smaller than that calculated for many of the isothermal holds. In the absence of turbulent flow and with the shallower hydrostatic tension, these conditions are far less favorable for dynamic nucleation. Indeed, dynamic nucleation was not observed in any of the free-cooling cycles.

4. Discussion

At sub-critical undercooling levels, classical nucleation theory predicts that the melt should remain liquid well beyond the observation time, such that no cycles would be expected to solidify during these experiments. However, these experiments showed the sample to consistently solidify at moderate undercooling levels. Several mechanisms for solidification within the framework of classical nucleation theory have been considered, including contact with a solid particle or chemical contamination; however, these are not consistent with our experimental observations.

Within classical nucleation theory, heterogeneous nucleation on a solid–liquid interface reduces the required volume, and, therefore, the energy barrier, to form a supercritical nucleus. By reducing the energy barrier, solidification can occur at sub-critical undercoolings; however, this nucleation mechanism requires a solid–liquid interface on which nuclei may form. In containerless processing, such an interface would require solid particles in the sample chamber to impact the sample. In EML, such solid particles may occur as either “dust” or as larger “flakes”. Dust clouds may form in EML by the condensation of evaporated material and are often dense enough to be visible during experimental

processing [30]. However, such evaporation and condensation can only occur in a gas atmosphere. The presence of such “dust” was not possible in these experiments, as they were conducted in vacuum. In vacuum, any evaporated material travels radially away from the sample until it reaches a solid surface. The surfaces in the levitation chamber of the ISS-EML are cold enough for the evaporated material to condense. Evaporation in a vacuum results in a coating formed via physical vapor deposition on the sample chamber, EML coils, sample holder, etc., but does not cause the formation of “dust”.

Upon reaching a thickness in the order of 10 μm , the accumulated coating deposited on the inside of the EML chamber can separate and produce “flakes” [31]. The operating plan for the ISS-EML, including limits on experiments, is designed to prevent these flakes from forming. While larger “flakes” of material have been documented [31], such larger “flakes” are very rare in EML and are, therefore, very unlikely to account for the large number of solidification events observed during this series of experiments. Further, no large “flakes” were observed during these experiments.

Chemical contamination has been suggested as a possible explanation for the observed solidification behavior. If chemical contamination were present as a mechanism to reduce the energy barrier to nucleation, the accessible undercooled region would have been greatly reduced. The presence of dissolved oxygen within a sample could also serve to reduce the accessible undercooled region by providing additional heterogeneous nucleation sites. However, solid zirconium oxide does not form until a very high concentration of oxygen is present. Instead, any oxygen is dissolved into solution within the metallic phase. While oxygen is known to stabilize the crystal phase, its presence could cause a small increase in the melting temperature of the sample. Precipitates could affect the accessible undercooling such that the maximum achievable undercooling could be reduced.

To test for changes in chemical composition, the sample was free-cooled before, during, and after the experiment series. In this experiment series, the sample was observed to undercool by over 300 K below the melting temperature. Such deep levels of undercoolings would not be observed if the sample were sufficiently contaminated to provide mechanisms for solidification at these sub-critical undercooling levels.

The remaining hypothesis, then, is that dynamic nucleation occurs as a result of flow effects within the melt. During these experiments, the sample remained liquid for less than 600 s at sub-critical undercoolings. During these isothermal holds, the magnetohydrodynamic forces drove rapid, sustained stirring in the sample. The deepest hydrostatic tension generated by the flow in the samples was 235 Pa, which may be deepened by a similar factor by turbulent eddies. While the hydrostatic tension of the fluid flow is insufficient to nucleate new voids in the melt, it is enough to excite existing voids that encounter the low-pressure region, as is required for dynamic nucleation.

Comparison with Prior Experiments Using Sustained Rapid Flow

Dynamic nucleation is consistent with the experimental results of this work and prior experiments on pure zirconium. This nucleation mechanism enables the conditions necessary for these instances of spontaneous nucleation. Both Zr and Zr-2.5Nb have very high melting temperatures, which permitted the samples to be held at deep levels of undercooling while large EML forces drove rapid stirring in the melt. In prior work, pure zirconium solidified during 18 of 19 cycles at sub-critical undercoolings [22]. The time to nucleation across various undercooling levels is plotted as a function of the fraction of maximum undercooling alongside the measurements on Zr-2.5Nb in Figure 4.

The data were analyzed for temperature dependence using a linear regression of the hold times as a function of undercooling. For the Zr-2.5Nb measurements, the slope of the linear regression was -102 ± 87 s; meanwhile in the regression of pure zirconium,

the slope was -115 ± 174 s. In both analyses, the uncertainty in the slope is comparable in magnitude to the fit and is, therefore, not statistically significantly different from zero. As a result, the uncertainties suggest that the hold times are not directly dependent on temperature in either pure zirconium or in Zr-2.5Nb. This lack of dependence is consistent with the stochastic nature of dynamic nucleation. Instead, the sample must wait for a sufficiently large pressure change to provide the local undercooling that would trigger solidification. Once sufficient undercooling is achieved for the shock-induced nucleus to grow, further undercooling would have no effect. The shock is expected to be large enough that solidification would progress for any undercooling.

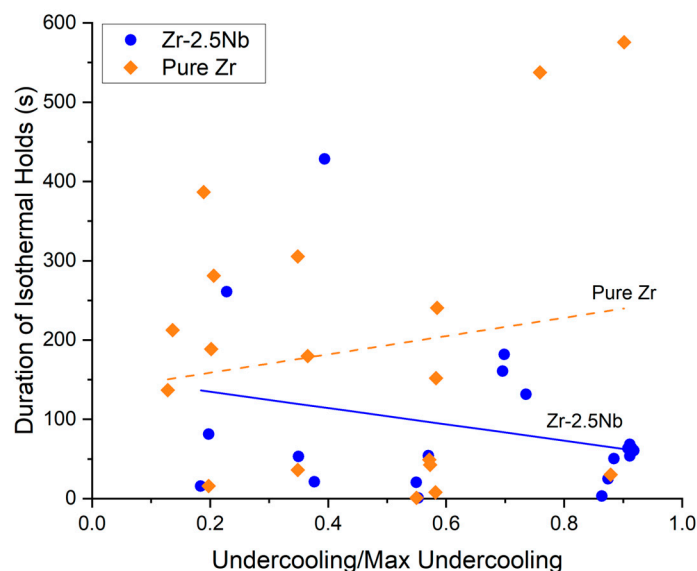


Figure 4. Both Zr and Zr-2.5Nb experienced spontaneous solidification events while the undercooled melt was held in isothermal conditions. The times for which the samples were held are plotted at the different undercoolings. Linear regressions were used to evaluate the temperature dependence of the hold times on undercooling; however, the slopes were -102 ± 87 s for Zr-2.5Nb and -115 ± 174 s for pure zirconium. With such large deviations, the slopes are not statistically different from zero, suggesting the hold times are not directly dependent on temperature.

In absence of significant temperature effects, the hold times between the different experiments were considered. During the isothermal holds, Zr-2.5Nb solidified after an average of 89.9 ± 103 seconds, whereas the pure zirconium sample required 190 ± 176 s for solidification to occur. A two-sample t-test [32] was used to statistically compare the mean hold times between the zirconium and Zr-2.5Nb. If the variance in the data is assumed to be equal, the t-statistic for these data sets is -2.11, which indicates a significant difference between the mean values of the two populations. Further, the *p*-value is 0.04, which signifies a strong statistical significance. These results statistically support the observed difference in hold times between pure zirconium and Zr-2.5Nb to be significant.

Both the pure zirconium and Zr-2.5Nb samples deeply undercooled. While the Zr-2.5Nb sample was undercooled more deeply (by about 10 degrees or 2.8% of the maximum undercooling) than the pure zirconium sample in several cycles, the range of flow conditions between these samples were very similar. The results of these experiments are outlined in Table 1. Since the Zr-2.5Nb sample was more deeply undercooled, the melt viscosity was higher during these isothermal holds and resulted in slower flow speeds, slightly lower Reynolds numbers (but still above the laminar–turbulent transition), and slightly less flow-induced hydrostatic tension. Despite the slower flow conditions in the Zr-2.5Nb experiments, the sample solidified quicker, on average, than in the pure zirconium experiments. The data suggests that the hold time to the formation of a supercritical cluster

is not directly dependent on the undercooling, nor is it directly dependent on the flow conditions within the melt.

Table 1. A comparison of the experimental results and conditions between the experiments on pure Zr and Zr-2.5Nb.

	Pure Zirconium	Zr-2.5Nb
Solidification Events within 600 s	18/19	20/20
Observed Maximum Undercooling [K]	321	305
Undercooling at Isothermal Holds [K]	45–290	54–302
Flow Speed [cm/s]	13.7–20.9	13.8–19.4
Reynolds Number	987–1900	990–1690
Maximum Hydrostatic Tension [Pa]	140–263	137–235

Dynamic nucleation is the subject of several planned experiments in the ISS-EML facility. The effects of external pressure on dynamic nucleation will be further explored through processing in an inert gas environment. Additional experiments have also been selected for processing in the ISS-EML to investigate samples of a lower melting temperature, which will permit experiments with less stirring during isothermal holds.

5. Conclusions

In the ISS-EML, a Zr-2.5Nb sample solidified within the experimental time frame at undercooling levels at which classical nucleation theory predicted the sample to remain liquid. In these experiments, the molten sample was held at moderate undercooling levels for up to 600 s, and in all 20 observations, the sample solidified within the observation window. While this behavior is not consistent with classical nucleation theory, it is consistent with prior experiments in which a pure zirconium sample solidified in 18 of 19 observations at moderate undercoolings at which the sample was expected to remain liquid. The time until solidification between the two samples was analyzed and it was found that the Zr-2.5Nb sample solidified, on average, almost 100 s quicker than the pure zirconium sample while at similar flow conditions. Both sets of experiments, while inconsistent with classical nucleation theory, are consistent with dynamic nucleation.

Author Contributions: G.P.B. planned and directed experiments, analyzed the results, analyzed the models, prepared and edited the manuscript. S.S., M.B. and S.N. prepared and planned for science operations and operated the experimental facility. The sample was proposed and prepared for operations by M.M. R.W.H. planned and directed experiments, provided input for analysis, and edited and reviewed the manuscript. All authors have read and agreed to the published version of the manuscript.

Funding: Partial support for personnel on this project was provided through DLR/DAAD Research Fellowships for Postdocs Program Number 57622550. Support for this project was provided to the USTIP project through NASA Grants NNX16AB40G, 80NSSC21K0103, and 80NSSC24K1274. M.M. acknowledges funding from the ESA MAP project ThermoProp (AO-099-022) and funding from the DLR Space Administration with funds provided by the Federal Ministry for Economic Affairs and Climate Action (BMWK) under Grant No. 50WM1759.

Data Availability Statement: The experimental data presented in this study is expected to be openly available in the ESA Human and Robotic Exploration Data Archive following completion of ISS-EML Batch 3 operations and sample download. Modeling data will be included in the USTIP Project for Batch 3 Operations in the NASA Physical Sciences Informatics system following completion of ISS-EML Batch 3 operations and sample download.

Acknowledgments: The authors acknowledge collaborate support by team members from the Microgravity User Support Center (MUSC) through access to the ISS-EML facility which is a joint undertaking of the European Space Agency (ESA) and the German Aerospace Administration (DLR). The authors furthermore thank Isabelle Crassous, Framatome, for the supply of the Zr-2.5Nb sample material. This research was performed using computational resources supported by the Academic & Research Computing group at Worcester Polytechnic Institute.

Conflicts of Interest: On behalf of the authors, the corresponding author states that there are no conflicts of interest.

Abbreviations

The following abbreviations are used in this manuscript:

EML	Electromagnetic Levitation
ESL	Electrostatic Levitation
CFD	Computational Fluid Dynamics
ISS-EML	International Space Station Electromagnetic Levitator

Appendix A. Magnetohydrodynamic Model

Magnetohydrodynamic modeling is used to calculate the flow conditions within a molten electromagnetic levitation (EML) sample. In this model, the distribution of the magnetic forces relies on a discretization of the induced electromagnetic currents within the sample. These electromagnetic currents are calculated using the volume integral method coupled with the method of mutual inductances evaluated on a discretized representation of the sample, as is described by [33,34] with corrections in [35]. The Lorentz forces are calculated from the current density and interpolated onto a computational fluid dynamics (CFD) mesh to define the body forces acting on the fluid. The model uses an axial-symmetric mesh to numerically solve the Navier–Stokes equations and calculate the flow within the sample. The boundaries of the system are defined such that flow cannot cross the symmetry boundary about the polar axis of the spherical sample, flow cannot cross the free surface of the drop, and derivatives must be zero at the symmetry boundary to maintain symmetry across the boundary. Additionally, the free surface of the drop is assumed to be free of traction and permits slip. The models presented here address flow conditions during isothermal holds in quasi steady-state conditions.

The magnetohydrodynamic model is validated against a rare physical case in which the melt separates into a two-phase liquid. The second phase enables particle velocimetry to be used to directly quantify the fluid flow. The results of that work are compared to the numerical model and show that the flow calculated by the model is within 7% of the observed velocities, which is less than the uncertainty of the particle velocimetry [36].

During the steady-state conditions of the isothermal holds, the electromagnetic field is dominated by the heater circuit, which results in a magnetic field referred to as “heater-dominated”. As a result, the flow pattern is also referred to as a heater-dominated flow. On the right-hand side of Figure A1, the typical distribution for applied magnetic forces in a heater-dominated field are plotted. The magnetic field is largest near the surface of the sample and along the equator. This distribution of forces drives the flow pattern shown on the left-hand side of Figure A1, which is a typical result for a “heater-dominated” flow. The flow pattern consists of two recirculating loops that flow into the sample at the equator. Additionally, the flow induces hydrostatic tension, given for this case in Figure A2. The deepest hydrostatic tension occurs along the surface of the sample where the flow is fastest. However, in the presence of turbulence, turbulent eddies may increase the local hydrostatic tension by a factor similar to the induced hydrostatic tension.

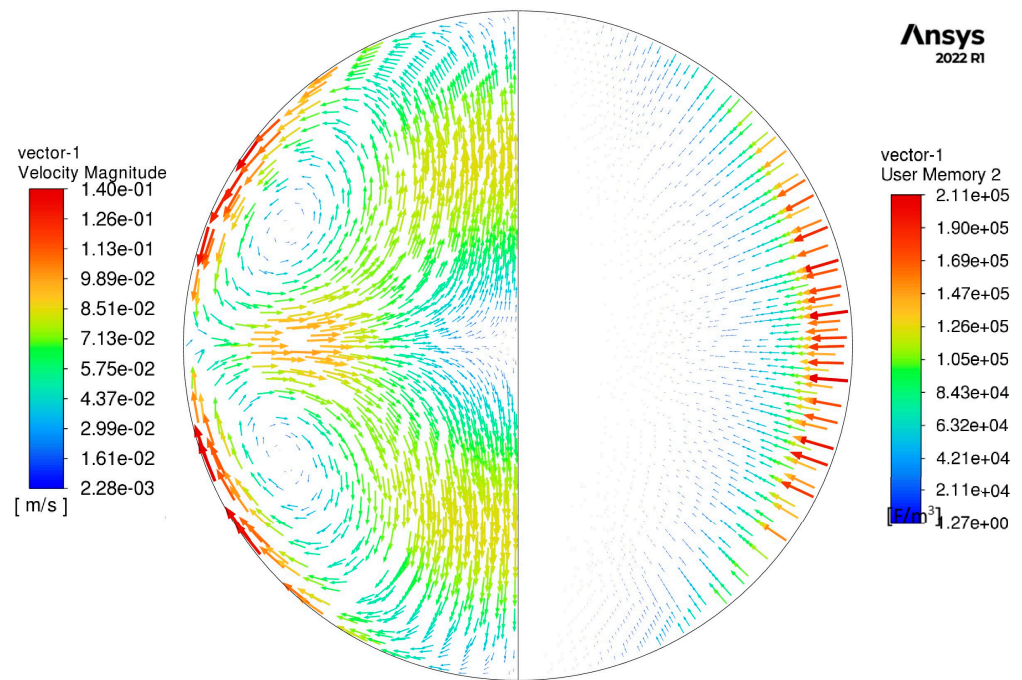


Figure A1. The velocity vectors (left) for the flow geometry during the isothermal hold at 255 K below the melting temperature. The fluid flow is driven by the electromagnetic forces (right) acting on the sample. In this case, the melt is flowing at a rate of 13.9 cm/s which corresponds to a Reynolds number of 975, indicating turbulent fluid flow which provides additional hydrostatic tension inside the turbulent eddies.

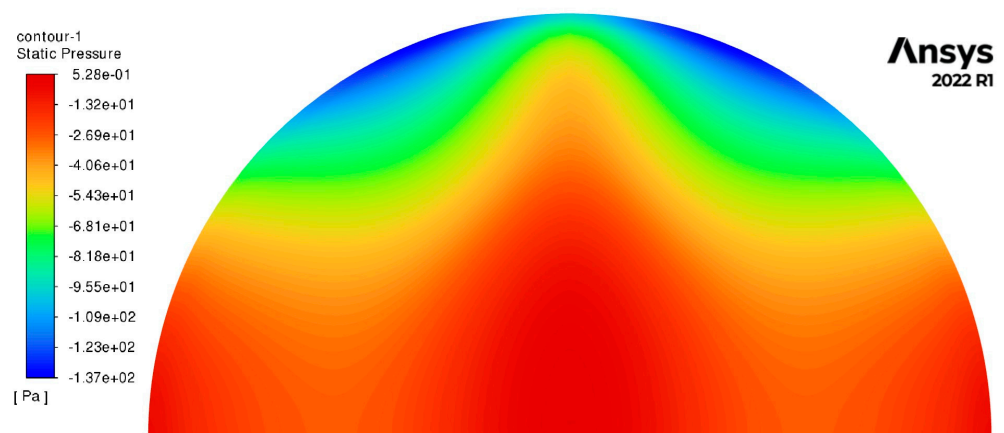


Figure A2. During the isothermal hold, the flow within the drop induces hydrostatic tension. During cycle 46, the isothermal hold was maintained at 255 K below the melting temperature and the deepest tension is 137 Pa at the surface of the sample where the flow is fastest. It is within these regions of deepest hydrostatic tension that the voids are most likely to be excited.

References

1. Egry, I. Structure and properties of levitated liquid metals. *J. Non-Cryst. Solids* **1999**, 250–252, 63–69. [\[CrossRef\]](#)
2. Herlach, D.M.; Binder, S.; Galenko, P.K.; Gegner, J.; Holland-Moritz, D.; Klein, S.; Kolbe, M.; Volkman, T. Containerless Undercooled Melts: Ordering, Nucleation, and Dendrite Growth. *Metall. Mater. Trans. A* **2015**, 46, 4921–4936. [\[CrossRef\]](#)
3. Herlach, D.M. Dendrite Growth Kinetics in Undercooled Melts of Intermetallic Com-pounds. *Crystals* **2015**, 5, 355–375. [\[CrossRef\]](#)
4. Binder, S.; Kolbe, M.; Klein, S.; Herlach, D.M. Solidification of tetragonal Ni₂B from the undercooled melt. *EPL* **2012**, 97, 36003. [\[CrossRef\]](#)
5. Rodriguez, J.E.; Matson, D.M. Lateral heat flux and remelting during growth into the mushy-zone. *Acta Mater.* **2017**, 129, 408–414. [\[CrossRef\]](#)

6. Strohmenger, J.; Volkmann, T.; Gao, J.; Herlach, D.M. The formation of a metastable peritectic phase in Nd–Fe–B alloys investigated by in situ X-ray diffraction during solidification. *Mater. Sci. Eng. A* **2006**, *413–414*, 263–266. [\[CrossRef\]](#)
7. Matson, D.M.; Battezzati, L.; Galenko, P.K.; Gandin, C.-A.; Gangopadhyay, A.K.; Henein, H.; Kelton, K.F.; Kolbe, M.; Vallotton, J.; Vogel, S.C.; et al. Electromagnetic levitation containerless processing of metallic materials in microgravity: Rapid solidification. *npj Microgravity* **2023**, *9*, 65. [\[CrossRef\]](#)
8. Cao, C.D.; Herlach, D.M.; Kolbe, M.; Görler, G.P.; Wei, B. Rapid solidification of Cu₈₄Co₁₆ alloy undercooled into the metastable miscibility gap under different conditions. *Scr. Mater.* **2003**, *48*, 5–9. [\[CrossRef\]](#)
9. Bracker, G.P.; Schneider, S.; Wunderlich, R.; Fecht, H.; Zhao, J.; Hyers, R.W. Confirmation of Anomalous Nucleation in Zirconium. *JOM* **2020**, *72*, 3140–3146. [\[CrossRef\]](#)
10. Lohöfer, G.; Xiao, X. Residual fluid flow in liquid metallic droplets processed in the space station electromagnetic levitation facility. *Phys. Fluids* **2022**, *34*, 077114. [\[CrossRef\]](#)
11. Egry, I.; Brooks, R.; Holland-Moritz, D.; Novakovic, R.; Matsushita, T.; Plevachuk, Y.; Ricci, E.; Seetharaman, S.; Sklyarchuk, V.; Wunderlich, R. Thermophysical properties of liquid Al–Ni alloys. *High Temp.-High Press.* **2010**, *38*, 343–351.
12. Reiplinger, B.; Brillo, J. Density and excess volume of the liquid Ti–V system measured in electromagnetic levitation. *J. Mater. Sci.* **2022**, *57*, 7954–7964. [\[CrossRef\]](#)
13. Champdoizeau, Q.; Vallotton, J.; Henein, H. Thermophysical Properties Measurement of Al–22.5 wt pctCu in Reduced Gravity Using the ISS-EML. *Metall. Mater. Trans. A* **2023**, *54*, 4151–4158. [\[CrossRef\]](#)
14. Turnbull, D. Formation of Crystal Nuclei in Liquid Metals. *J. Appl. Phys.* **1950**, *21*, 1022–1028. [\[CrossRef\]](#)
15. Porter, D.A.; Easterling, K.E.; Sherif, M.Y. Solidification. In *Phase Transformations in Metals and Alloys*, 3rd ed.; CRC Press: New York, NY, USA, 2009; pp. 189–260.
16. Morton, C.W.; Hofmeister, W.H.; Bayuzick, R.J.; Rulison, A.J.; Watkins, J.L. The kinetics of solid nucleation in zirconium. *Acta Mater.* **1998**, *46*, 6033–6039. [\[CrossRef\]](#)
17. Hyers, R.W.; Zhao, J.; Bracker, G.P.; Wunderlich, R.; Fecht, H. Anomalous Nucleation in Undercooled Melts Processed by Electromagnetic Levitation. In *Light Metals*; Springer: Cham, Switzerland, 2019. [\[CrossRef\]](#)
18. Hofmeister, W.H.; Bayuzick, R.J.; Hyers, R.W.; Trapaga, G. Cavitation-induced nucleation of zirconium in low earth orbit. *Appl. Phys. Lett.* **1999**, *74*, 2711–2713. [\[CrossRef\]](#)
19. Smirnova, D.E.; Starikov, S.V.; Gordeev, I.S. Evaluation of the structure and properties for the high-temperature phase of zirconium from the atomistic simulations. *Comput. Mater. Sci.* **2018**, *152*, 51–59. [\[CrossRef\]](#)
20. Hunt, J.D.; Jackson, K.A. Nucleation of Solid in an Undercooled Liquid by Cavitation. *J. Appl. Phys.* **1966**, *37*, 254–257. [\[CrossRef\]](#)
21. Frawley, J.J.; Childs, W.J. Dynamic Nucleation Supercooled Metals. *Trans. Metall. Soc. AIME* **1968**, *242*, 256–263.
22. Bracker, G.P.; Schneider, S.; Matson, D.M.; Hyers, R.W. Dynamic nucleation in sub-critically undercooled melts during electromagnetic levitation. *Materialia* **2022**, *26*, 101623. [\[CrossRef\]](#)
23. Shima, A.; Sakai, I. On the equation for the size distribution of bubble nuclei in liquids (Report 2). In *Reports of the Institute of High Speed Mechanics*; Institute of High Speed Mechanics: Sendai, Japan, 1987; Volume 54, pp. 51–59.
24. Schneider, S.; Institute for Materials Physics in Space, German Aerospace Center (DLR), Köln, 51147, Germany. Private communication, 2022. EML Flight Samples Certificates and Paper Documentation: Sample #94, Zr-2.5Nb-0.11O.
25. Lohöfer, G. Device for Positioning and Melting Electrically Conductive Materials Without a Receptacle. US Patent 4993043A, 12 February 1991. Available online: <https://patents.google.com/patent/US4993043A/en> (accessed on 25 July 2025).
26. Lohöfer, G.; Piller, J. The new ISS Electromagnetic Levitation Facility—MSL-EML. In *40th AIAA Aerospace Sciences Meeting & Exhibit, Reno, NV, USA, 14–17 January 2002*; American Institute of Aeronautics and Astronautics: Reston, VA, USA, 2012. [\[CrossRef\]](#)
27. Seidel, A.; Soellner, W.; Stenzel, C. EML—An electromagnetic levitator for the International Space Station. *J. Phys. Conf. Ser.* **2011**, *327*, 012057. [\[CrossRef\]](#)
28. Paradis, P.-F.; Rhim, W.-K. Thermophysical properties of zirconium measured using electrostatic levitation. In *Proceedings of the SPIE's International Symposium on Optical Science, Engineering, and Instrumentation, Denver, CO, USA, 18–23 July 1999*; Ramachandran, N., Ed.; SPIE: Bellingham, WA, USA, 1999; p. 292. [\[CrossRef\]](#)
29. Hyers, R.W.; Trapaga, G.; Abedian, B. Laminar-turbulent transition in an electromagnetically levitated droplet. *Metall. Mater. Trans. B* **2003**, *34*, 29–36. [\[CrossRef\]](#)
30. Fromm, E. Reduction of metal evaporation losses by inert gas atmospheres. *Metall. Trans. A* **1978**, *9*, 1835–1838. [\[CrossRef\]](#)
31. Nawer, J.; Stanford, B.; Kolbe, M.; Schneider, S.; Gossé, S.; Wunderlich, R.K.; Mohr, M.; Borzi, A.; Neels, A.; Matson, D.M. Thermodynamic assessment of evaporation during molten steel testing onboard the International Space Station. *npj Microgravity* **2024**, *10*, 77. [\[CrossRef\]](#)
32. Montgomery, D.C.; Runger, G.C.; Hubele, N.F. Chapter 5: Decision Making for Two Samples. In *Engineering Statistics*, 5th ed.; John Wiley & Sons, Incorporated: Hoboken, NJ, USA, 2011; pp. 230–297.

33. Zong, J.-H.; Szekely, J.; Schwartz, E. An improved computational technique for calculating electromagnetic forces and power absorptions generated in spherical and deformed body in levitation melting devices. *IEEE Trans. Magn.* **1992**, *28*, 1833–1842. [[CrossRef](#)]
34. Lohöfer, G. Force and torque of an electromagnetically levitated metal sphere. *Q. Appl. Math.* **1993**, *51*, 495–518. [[CrossRef](#)]
35. Hyers, R.W. Modeling of and Experiments on Electromagnetic Levitation for Materials Processing. Ph.D. Thesis, Massachusetts Institute of Technology, Cambridge, MA, USA, 1998.
36. Lee, J.; Matson, D.M.; Binder, S.; Kolbe, M.; Herlach, D.; Hyers, R.W. Magnetohydrodynamic Modeling and Experimental Validation of Convection Inside Electromagnetically Levitated Co-Cu Droplets. *Metall. Mater. Trans. B* **2014**, *45*, 1018–1023. [[CrossRef](#)]

Disclaimer/Publisher’s Note: The statements, opinions and data contained in all publications are solely those of the individual author(s) and contributor(s) and not of MDPI and/or the editor(s). MDPI and/or the editor(s) disclaim responsibility for any injury to people or property resulting from any ideas, methods, instructions or products referred to in the content.